ULTIMATE DEFORMATION CAPACITY OF UNBONDED POST-TENSIONING MONOSTRAND ANCHORAGES UNDER MONOTONIC AND HIGH-AMPLITUDE CYCLIC LOADING

Luis A. BEDRIÑANA — **Doctor candidate, Kyoto University**
Kaiwei ZHANG — **Graduate student, Kyoto University**
Katsuhito OSHIMA — **Senior Engineer, Sumitomo (SEI) Steel Wire Corp.**
Minehiro NISHIYAMA — **Professor, Kyoto University**

Abstract: This paper presents the principal results of an experimental investigation on the ultimate behavior of monostrand post-tensioning anchorages subjected to high-amplitude cyclic loads. In addition, this paper addresses the influence of anchorage type, loading pattern and strand size on the ultimate capacity of the anchorages. Specimens consisted of monostrands assembled with anchorages at both ends. Two types of commercially available anchorages were tested. The results showed that ultimate displacement capacity of the strands were limited by fracture of some wires inside the anchorages, with strains as low as 1.42%.

Keywords: anchorage, unbonded, post-tensioning, monostrand, cyclic loading, self-centering.

1. INTRODUCTION

During the last decades, there has been an increasing interest in applying unbonded post-tensioned (PT) precast concrete (PCa) structures in seismic regions to control residual damage [1]. Unbonded PT anchorage systems have been largely used in PCa members subjected to service load, but their application as earthquake-resistant members is not well documented. Moreover, it was noted that cyclic loading on unbonded PT strand-anchorage systems might cause premature failure of strands inside anchorages [2,3]. Consequently, further research is needed on unbonded PT anchorages for their seismic applications expected to meet performance-based criteria.

This paper describes the results of an experimental evaluation of the behavior and failure mechanism of monostrand anchorages subjected to cyclic loads. In addition, this paper addresses the influence of high-amplitude low-frequency loading on the elongation capacity of strand-anchorage at fracture.

2. OVERVIEW OF THE EXPERIMENT

Test specimens consisted of monostrands assembled with anchorages at both ends. Table 1 describes the configurations used in the test. Seven-wire PT monostrands, with diameters of 12.7 and 15.2mm were considered. The nominal fracture loads (F_{pu}) of the strands were 183 and 261kN for the 12.7 and 15.2-mm strands, respectively. The nominal cross-sectional areas were 98.7 and 138.7mm^2 for the 12.7 and 15.2-mm strands, respectively. The measured breaking loads ($F_{pu,m}$), as reported in the mill sheet, were 197 and 278kN for the 12.7 and 15.2-mm strands, respectively. Figure 1 shows details of the anchorages used in this test. Two types of monostrand anchorage were studied: single-use grip barrel anchor (BL) and casting plate anchor (CP). Generally, CP anchors are made from grey ductile cast iron, whereas BL anchors are manufactured from high carbon steel. The difference of materials on the two types of anchorage produces different hardness of the interior surface (where wedges are located), which may lead to different gripping conditions of the wedges. The sizes of these anchorages corresponded to the size of strand used (Table 1). In addition, two-piece (referred to as 2P herein) and three-piece (referred to as 3P herein) wedges were used. It is important to note that 2P wedges had vertical slits at the top part (Fig. 1) and the 3P wedges were used with a binding ring at the top part, which helps in reducing differential setting by holding the pieces together. All test samples were obtained from one manufacturer.

Figure 2 presents the general test setup, in which tensile loads were applied by a 300 kN-capacity servo-hydraulic computer-controlled material testing system. Steel plates were attached to the testing machine to enable installation of strands and anchorages. Vertical alignment of specimens was carefully checked during the entire installation process and no initial preload was applied to the anchorages. The anchor to anchor length (L_{ps}) was about 1060 and 1065 mm for specimens with BL and CP anchorages, respectively. As for the measurement systems, four strain gauges and three linear variable displacement transducers (LVDT) were used in each of the specimens, as can be seen in Fig. 2. The central LVDT was fixed to the steel loading plates to capture total elongations and the other two LVDT were attached at each anchorage zone to measure relative movement of strands into the anchorages. The strain gauges were attached along a single wire's axis (i.e. with a slight angle

from vertical axis) at a distance of 50mm from top and bottom anchorages (Fig. 2). In addition to this instrumentation, load and ram cylinder displacement from the testing machine were recorded.

Table 2 shows all loading cases applied to each of the anchorage's configurations shown in Table 1. Three samples were tested for each combination of configuration and loading condition, giving a total of 84 specimens for this study. For the M loading case, monotonic tensile load was applied at a constant strain rate of 0.02 mm/mm/min, in accordance with the ICC-ES document [4]. Furthermore, six conditions of cyclic loads (L1-L6) were applied in which the loading protocol consisted of three parts: (1) increasing load up to a level of F_{ave} (average of the upper and lower limit), (2) main cyclic part, in which at least 200 cycles of sinusoidal loads were applied at a given frequency and within a defined amplitude (F_{min} to F_{max}), and (3) increasing monotonic load up to fracture of any individual wire. This loading protocol is a modification of protocols used by other researchers [5]. The loading cases shown in Table 2 were selected to introduce inelastic deformations in the strands as well to produce drastic changes of stress into specimens, to simulate seismic conditions. The maximum frequency (4Hz) and load ($0.95F_{pu}$) applied to the specimens were larger than specified values in current test requirements [4,6].

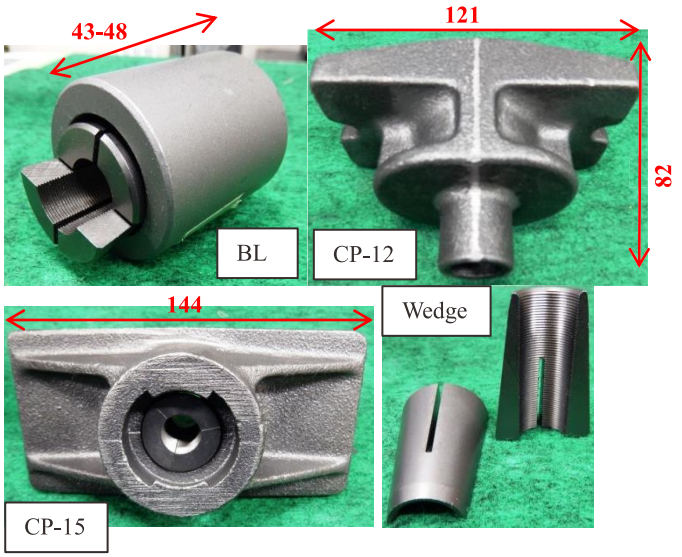

Fig. 1 Anchorage types used in the test (units: mm)

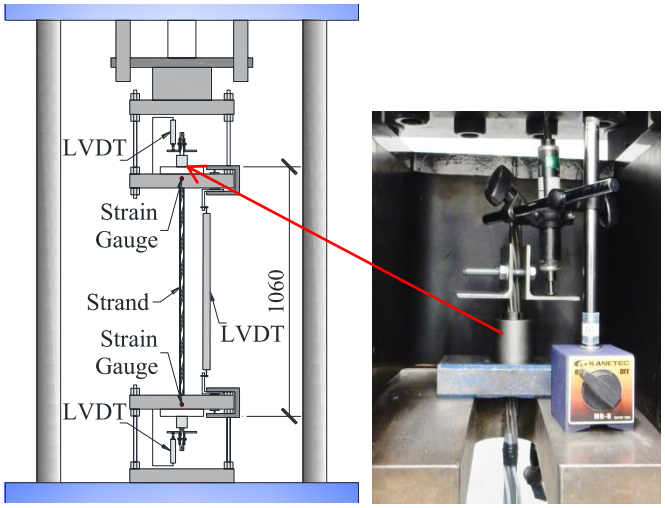

Fig. 2 View of the test setup (units: mm)

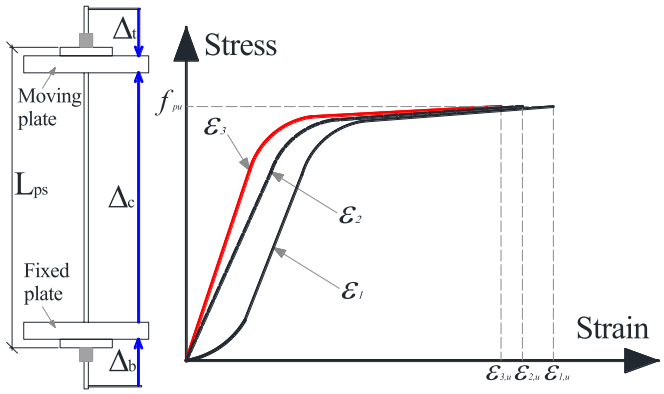

Fig. 3 Definitions of stress-strain curves

Table 1 Test Matrix.

Strand Diameter (mm)	Anchor Type	Wedge Type
12.7	BL	2P
	CP	2P
15.2	BL	2P
	CP	3P

3. TEST RESULTS AND DISCUSSION

Even though the three transducers and four strain gauges used in the test captured deformations of strands, the information they conveyed was different. As shown in Fig.3, the central LVDT provides total elongation of strands (where total strain is given as $\varepsilon_1=\Delta_c/L_{ps}$) including the effects of anchorage seating, whereas the top and bottom LVDT captured relative movements of strands into anchorages. Then, engineering strand strains (given as $\varepsilon_2= [\Delta_c - \Delta_t - \Delta_b]/L_{ps}$) were calculated by removing wedge seating from total elongations. In addition, local strains of individual wires were captured by the strain gauges and reported in this paper as ε_3.

Raw data obtained from the measurement system were processed and adjusted as follows. First, the elastic modulus, calculated as the slope of the best-fit line of data points within the range of $0.2\text{-}0.6f_{pu}$, was obtained from stress-strain curves plotted for the different types of strains ε_1, ε_2 and ε_3. During this process, one elastic modulus for each type of stress-strain curve was calculated. It is worth to note that measured data below $0.2f_{pu}$ were

neglected to eliminate inaccurate measurements. Then, the stress-strain curves were shifted along strain-axis so the curves start at zero strain. Furthermore, the yield strength was calculated as the stress offset of 0.2% plastic strain and the corresponding calculated elastic modulus.

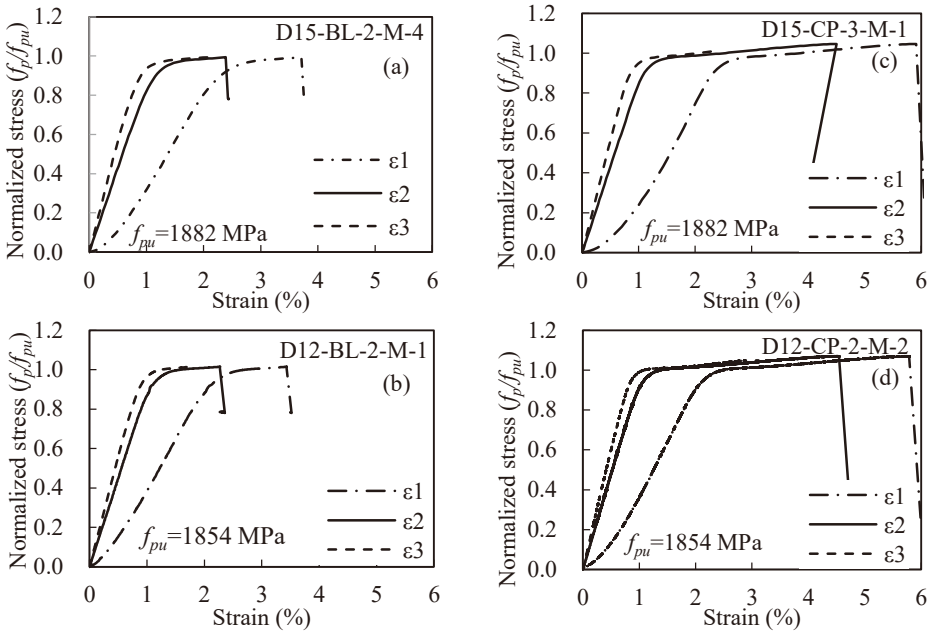

Fig. 4 Stress-strain curves under monotonic load

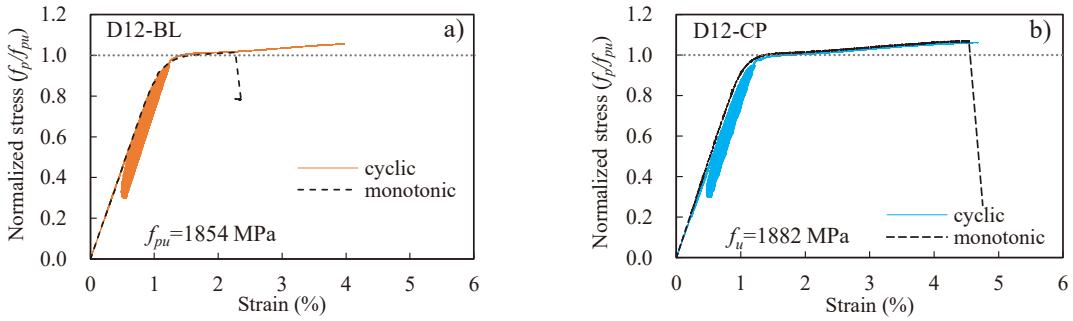

Fig. 5 Typical stress-strain curves under cyclic loading

3.1 Typical stress-strain curves

Figure 4 presents the different types of normalized stress-strain curves (f_p/f_{pu}-ε_p curve) obtained from four samples under monotonic loads. For each sample, it can be observed that the initial stiffnesses of the three types of curves were different, mainly because of the different information conveyed. As it was mentioned previously, ε_1 curve included the effect of anchorage seating and this influence was noticeable at the initial part of the curve where some nonlinearity was observed in all samples; consequently, this curve is not representative of the ultimate strain capacity of strand-anchorage systems. The influence of anchorage seating was then eliminated in the ε_2 curve, which gives a better representation of engineering strand strains and the ultimate deformation capacity. On the other hand, ε_3 curve was obtained directly from strain gauges, showing deformations of individual wire (material behavior) rather than of the strand. Since the engineering stress and strain of strands are important parameters for designing, the ultimate deformation capacity is reported from ε_2 curve hereinafter.

Figure 5 shows normalized stress－strain curves, corresponding to ε_2 definition, obtained from samples subjected to cyclic loading. In this figure, a monotonic stress-strain curve of one sample is also plotted for comparison. As it can be seen, the specimens were subjected to inelastic cyclic deformation, which extended above the proportionality limit of the stress-strain curves. Moreover, the initial and post yielding stiffness were similar for the cyclic and monotonic loading cases, despite the 200 inelastic strain cycles. Interestingly, it was found that the maximum deformation capacity of cyclically loaded specimen was about twice as large as the monotonic one for the 12.7-mm BL anchorage.

3.2 Ultimate deformation capacity

The ultimate stress and strain of specimens subjected to monotonic loading are shown in Fig. 6. The ultimate

stress was estimated from the breaking load and nominal section, while the ultimate strain was taken from of ε_2 curve. According to the results, all samples had an ultimate stress larger than $0.95f_{pu}$, complying with AIJ [6]. In addition, CP anchors were able to maintain slightly higher ultimate stress than BL anchors. The ultimate deformation capacity for all samples was limited by the fracture of few outer wires inside the anchorage zone; therefore, full capacity of strands was not developed. Moreover, some samples of BL anchorages showed ultimate strains less than 2%, while all CP samples had ultimate strains larger than 4%. As for the influence of strand diameter, 12.7-mm strands showed larger, about two times in average, ultimate strain than 15.2-mm strands.

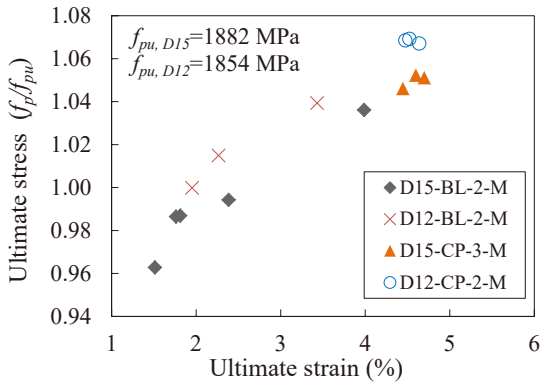

Fig. 6 Stress-strain curves under monotonic load

Table 2 Loading cases.

Code	F_{min} / F_{pu}	F_{max} / F_{pu}	Frequency (Hz)
M	-	-	-
L1	0.40	0.95	3
L2	0.50	0.90	3
L3	0.40	0.95	1
L4	0.50	0.90	1
L5	0.30	0.95	3
L6	0.50	0.95	4

Figure 7 shows the influence of loading frequency and amplitude on the ultimate capacity for specimens subjected to cyclic loading. CP anchorages reported about 1.8 times larger average ultimate strain capacity than BL anchorages for 15.2-mm specimens. It was also observed that some specimens of 15.2-mm BL anchorages had an ultimate strain capacity smaller than 2%. As for the 12.7-mm specimens, the CP anchorages also showed larger ultimate strain capacity than BL anchorages; however unlike 15.2-mm strand specimens, all 12.7-mm specimens had ultimate strain capacities over 2% and ultimate stresses over $1.0f_{pu}$. In addition, it was noted that 15.2-mm specimens subjected to 1Hz loading reported the lowest deformation capacity (about 1.42%). Conversely, the frequency showed no significant influence on the ultimate strain capacity of CP anchorage for neither 12.7-mm nor 15.2-mm specimens. It is worth to mention that the ultimate strain capacity of BL anchorages showed larger scatter than CP anchorages, which should be taken into account during the seismic design.

As it was mentioned before, three types of cyclic loading amplitudes were applied to the specimens: *A1* from 0.50 to $0.90f_{pu}$, *A2* from 0.40 to $0.95f_{pu}$, and *A3* from 0.30 to $0.95f_{pu}$. It was observed that the lowest deformation capacity was produced during the smallest amplitude *A1*, whereas *A3* reported the largest deformation capacity (3.86%) for 15.2-mm BL anchorages. As for 15.2-mm CP anchorages, the amplitude *A3* actually reported the lowest deformation capacity of about 3.65%. Unlike 15.2-mm specimens, 12.7-mm samples subjected to amplitudes *A1* and *A2* did not show noticeable differences on deformation capacity. Even though *A2* showed slightly larger ultimate strain values, no significant influence of loading amplitude was observed in 12.7-mm CP anchorages.

3.3 Wedge seating

Figure 8 shows the typical relationship between tensile load and wedge seating (Δ_t at the top and Δ_b at the bottom). The wedge seating under monotonic loads showed three stages: 1) rapid increase at low tensile load levels, 2) slower increase of movement as load increases, 3) slightly more rapid movements followed by fracture. In addition, BL anchorages showed smaller wedge seating at the ultimate stress than CP anchorages and 15.2-mm specimens showed larger wedge seating than 12.7-mm ones. The specimen subjected to cyclic loading sustained lower values of wedge seating than the monotonic loaded specimen; however, not clear influence of loading parameters on the wedge seating was found. Furthermore, once the desired amplitude of loading was reached, the wedges kept the same displacement until additional load was applied as can be seen in the horizontal lines in Fig. 8. After the cyclic loading was finished, small wedge seating was observed above the yielding load. It was also observed that 12.7-m specimens had smaller wedge seating at ultimate load than 15.2-mm specimens. In addition, the maximum wedge seating was about 7.5mm (0.71% of L_{ps}) for BL anchorage and 8.9mm (0.84% of L_{ps}) for CP anchorage. Although the influence of wedge seating was significant in the samples of this test, because a relatively short length (about 1m) was used, the wedge seating may be less significant in practical application with larger total strand lengths.

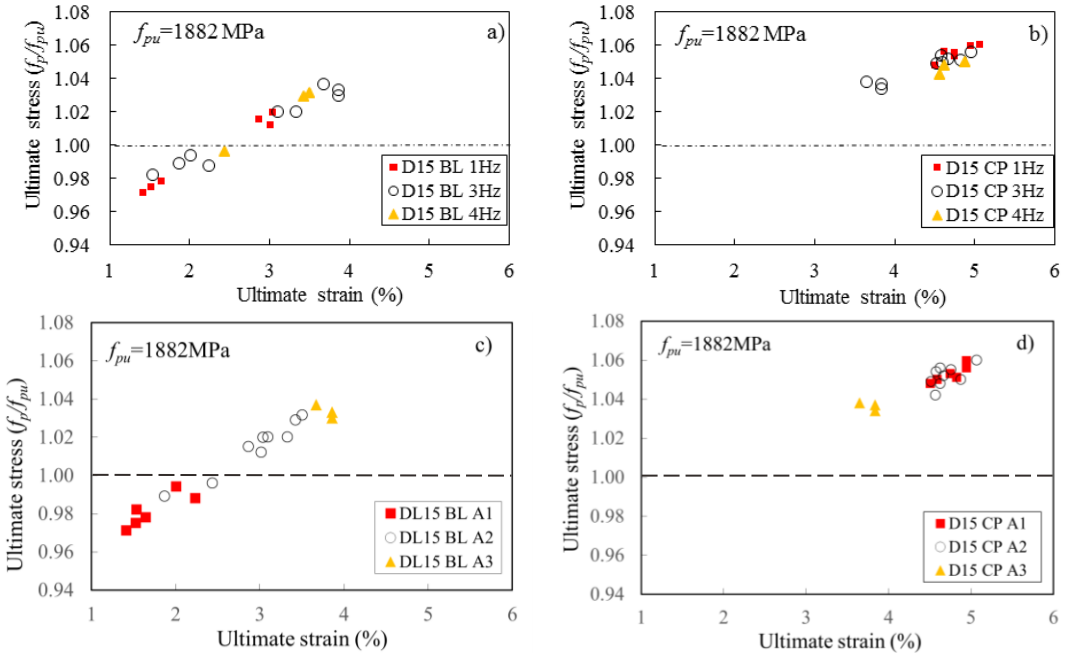

Fig. 7 Influence of frequency and amplitude loading on ultimate strain capacity

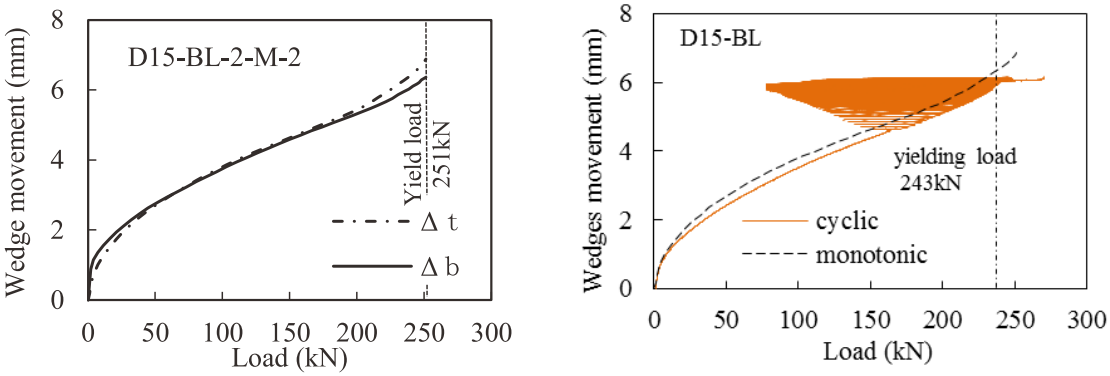

Fig. 8 Relationship between tensile load and wedge seating

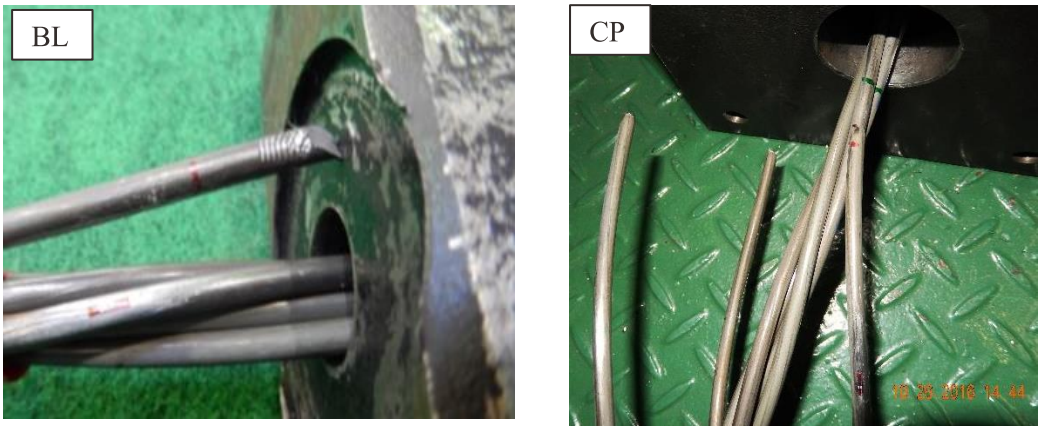

Fig. 9 Final state of specimens and failure types

3.4 Failure type of specimens

Figure 9 presents the final state of some specimens. Two different types of fractures were primarily observed: the diagonal cut of the section and a sort of necking of some outer wires. The former was mainly observed in BL anchorages, while the latter was mainly observed in CP anchorages. These types of fractures can be considered as an evidence of different failure mechanisms, which then leads to the differences in the ultimate strain and strength capacities. In addition, it was observed a correlation between the number of wires that fractured and the ultimate deformation capacity for most samples: the larger the fractured wires, the larger capacity was achieved. For

instance, the average number of fractured wires at failure was 1.4 and 3.7 for BL and CP anchorage, respectively. The relative movement of wedges inside anchorages induced localized stress concentration in outer wires of strands; moreover, since only the narrow part of wedges got in contact with the strands, no all the outer were gripped at the same time. This type of failure was observed in all the specimens with BL anchor, in whose cases, only one or few wire fractured first.

4. CONCLUSIONS

Based on the test results, the following conclusions can be drawn. All the samples showed ultimate stress larger than $0.95f_{pu}$, which complies with current standard requirements. The failure of the specimens occurred as a premature fracture of one or few strand wires inside the anchorages and two types of fractures were recognized: the diagonal cut of the section and a sort of necking of some outer wires. The former fracture type was mainly seen in BL anchorages, while the latter was mainly seen in CP anchorages. In addition, it was observed that no sample failed during the cyclic loading part of the protocol.

In general, CP anchors showed better ultimate strain capacity than BL anchors under the different loading cases. For monotonic loaded specimens, the ultimate strain capacity was found to be between 4.45-4.70% in CP and 1.51-3.99% in BL anchorages. As for the cyclic loaded specimens, the ultimate strain capacity ranged between 1.42 to 4.78% and 3.65 to 5.56% for BL and CP anchorage, respectively. The ultimate strain capacity of the samples was by far smaller than fracture strain of 6% to 7% commonly reported in mill sheets of monostrand. Moreover, deformation capacity of BL anchorage showed larger scatter than the one of CP.

Influence of loading frequency and amplitude was only found on the ultimate strain capacity of BL anchorages. In general, the influence of loading frequency and amplitude on the ultimate strain capacity was smaller in 12.7-mm specimens than in 15.2-mm ones. The maximum wedge seating was about 7.5mm (0.71% of L_{ps}) for BL anchorage and 8.9mm (0.84% of L_{ps}) for CP anchorage.

The conclusions drawn in this study provide a significant insight on the behavior of unbonded anchorages; however, they are valid only for the type of systems and for the loading conditions specified here. Therefore, further research is needed to explore the response of different anchorage systems and with different loading conditions.

ACKNOWLEDGMENTS

Financial support of the Peruvian National Council of Science, Technology, and Technological Innovation (CONCYTEC/CIENCIACTIVA) for the doctoral studies of the first author is acknowledged. Thanks to Sumitomo Steel Wire Corp. (SEI-SSW) for its generous contribution to this research by donating strand and anchorages. The authors recognize the kind support of Mr. Masato Yamada from SEI-SSW during the course of this research. All opinions, findings, and conclusions stated here are those of the authors and do not necessarily reflect the views of the supporting institutions.

REFERENCES

1. Kurama YC. Hybrid post-tensioned precast concrete walls for use in seismic regions. *PCI Journal* 2002; **47**(5): 36–59.
2. Weldon BD, Kurama YC. Nonlinear Behavior of Precast Concrete Coupling Beams under Lateral Loads. *Journal of Structural Engineering* 2007; **133**(11): 1571–1581.
3. Walsh KQ, Kurama YC. Behavior of unbonded post-tensioning monostrand anchorage systems under monotonic tensile loading. *PCI Journal* 2010; **55**(1): 97–117.
4. ICC-ES. *Acceptance Criteria for Post-tensioning Anchorages and Couplers of Prestressed Concrete (AC-303)*. Birmingham, AL: ICC Evaluation Service Inc.; 2011.
5. Musselman E, Fournier M, McAlpine P, Sritharan S. Behavior of unbonded post-tensioning monostrand anchorage systems under short duration, high amplitude cyclical loading. *Engineering Structures* 2015; **104**: 116–125.
6. AIJ. *Recomendations for Design and Construction of Partially Prestressed Concrete (Class III of Prestressed Concrete) Structures*. Tokyo: Architectural Institute of Japan (AIJ); 2003.